# Overview of the beam emission spectroscopy diagnostic system on the National Spherical Torus Experiment[a)]

D. R. Smith,[1,b)] H. Feder,[2] R. Feder,[2] R. J. Fonck,[1] G. Labik,[2] G. R. McKee,[1] N. Schoenbeck,[1] B. C. Stratton,[2] I. Uzun-Kaymak,[1] and G. Winz[1]
[1]*Department of Engineering Physics, University of Wisconsin-Madison, Madison, Wisconsin 53706, USA*
[2]*Princeton Plasma Physics Laboratory, Princeton, New Jersey 08543, USA*

(Presented 18 May 2010; received 17 May 2010; accepted 19 June 2010; published online 11 October 2010)

A beam emission spectroscopy (BES) system has been installed on the National Spherical Torus Experiment (NSTX) to study ion gyroscale fluctuations. The BES system measures $D_\alpha$ emission from a deuterium neutral heating beam. The system includes two optical views centered at $r/a \approx 0.45$ and 0.85 and aligned to magnetic field pitch angles at the neutral beam. f/1.5 collection optics produce 2–3 cm spot sizes at the neutral beam. The initial channel layout includes radial arrays, poloidal arrays, and two-dimensional grids. Radial arrays provide coverage from $r/a \approx 0.1$ to beyond the last-closed flux surface. Photodetectors and digital filters provide high-sensitivity, low-noise measurements at frequencies of up to 1 MHz. The BES system will be a valuable tool for investigating ion gyroscale turbulence and Alfvén/energetic particle modes on NSTX.
 [doi:10.1063/1.3478660]

## I. INTRODUCTION

A beam emission spectroscopy (BES) diagnostic system[1] has been installed on the National Spherical Torus Experiment (NSTX) (Ref. 2) to study ion gyroscale fluctuations. The system measures $D_\alpha$ emission ($n=3\rightarrow 2$ and $\lambda_0 = 656.1$ nm) from a deuterium neutral heating beam. The beam velocity and viewing geometry generate a Doppler shift that isolates neutral beam $D_\alpha$ emission from thermal $D_\alpha$ emission. $D_\alpha$ intensity fluctuations are proportional to ion density fluctuations with $\delta I/I = K\delta n_i/n_i$, where $K \approx 0.5$ is a weak function of plasma parameters. Measured and derived quantities from BES include density fluctuations, correlation lengths, decorrelation rates, mean flow rates, flow fluctuations, and particle flux. In addition, two-dimensional (2D) BES measurements provide fluctuation imaging and 2D flow fields.[3] BES measurements contribute to many research topics including ion temperature gradient and trapped electron mode turbulence, Alfvén/energetic particle modes, zonal flows, three-wave mode coupling, H-mode transition, and pedestal dynamics.[4]

Figure 1 shows the major components of a BES diagnostic system. Optical views are aligned to the magnetic field pitch angle within the neutral beam to optimize cross-field spatial resolution. To achieve sufficient $D_\alpha$ intensity, high-throughput optics with low f/# and high magnification are needed. The collection optics image the $D_\alpha$ emission field onto optical fibers for transmission to photodetectors. Collimating lenses and interference filters selectively pass neutral beam $D_\alpha$ emission and block thermal $D_\alpha$ emission. The photodetectors include photodiodes, transimpedance amplifiers, and frequency compensation circuits.[5,6] To reduce thermal noise and eliminate condensation hazards, photodetectors are cooled under vacuum. Finally, a digitizer with a finite impulse response filter inhibits high frequency amplifier noise from aliasing to lower frequency.

BES measurements on spherical torus (ST) devices, such as NSTX, present diagnostic challenges and scientific opportunities. To accommodate steep magnetic pitch angles inherent to ST plasmas, BES collection optics must view the neutral beam at steep, oblique angles. In addition, large pitch angle variation across the plasma limits the radial coverage of any single viewing geometry, so multiple viewing geometries are necessary for adequate coverage. The combination of neutral beam heating and low magnetic field in ST plasmas generates large equilibrium $E\times B$ flows. Turbulent eddies advect with $E\times B$ flow, so digitizer sampling rates in the megahertz range are necessary. However, gyroradii are larger at low magnetic field, so BES measurements in ST plasmas access higher normalized wavenumbers ($k_\perp \rho_s$) compared to measurements on conventional tokamaks. BES measurements can contribute to many ST physics topics including the role of low-$k$ fluctuations in anomalous momentum transport and validation of Alfvén/energetic particle mode models. This paper provides an overview of the NSTX BES diagnostic system.

## II. OPTICAL DESIGN

As shown in Fig. 2, the NSTX BES system employs a redshift viewing geometry and observes the neutral beam $D_\alpha$ full-energy manifold in the range of 659–662 nm. The redshift geometry provides better spatial resolution than the blueshift geometry over a wider radial range. However, the redshift geometry introduces carbon-II impurity lines at

[a)]Contributed paper, published as part of the Proceedings of the 18th Topical Conference on High-Temperature Plasma Diagnostics, Wildwood, New Jersey, May 2010.
[b)]Electronic mail: drsmith@engr.wisc.edu.

 

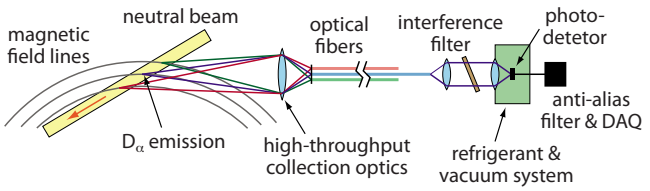


FIG. 1. (Color online) Diagram of a BES diagnostic system.

657.8 and 658.3 nm. Emission spectra from motional Stark effect[7] and fast ion $D_\alpha$ (Ref. 8) diagnostics indicate the C-II intensity is comparable to or less than the neutral beam $D_\alpha$ intensity with $I_{\mathrm{NB}\ D\alpha}/I_{\mathrm{C\text{-}II}} \approx 1-10$.

For adequate radial coverage and pitch angle matching, the BES system employs two optical views. As shown in Fig. 3, the inboard view, known as "R130," is centered at $R=130$ cm and $r/a \approx 0.45$. The outboard view, known as "R140," is centered at $R=140$ cm and $r/a \approx 0.85$. Note that $r/a$ values depend upon the particular plasma equilibrium. As described below, the views provide radial coverage from $r/a \approx 0.1$ to beyond the last-closed flux surface. Collection optics sits below the equatorial midplane and views upward into the neutral beam. To match typical NSTX pitch angles depicted in Fig. 2, R130 optics views the neutral beam at 26° with respect to the midplane, and R140 optics views the neutral beam at 37°.

R130 and R140 collection optics are identical with three-element, 11 cm diameter lens assemblies. The front surfaces of the lens assemblies are 80–100 cm from the middle of the neutral beam, and the back surfaces are 13–14 cm from the fiber faces. The lens assemblies demagnify the plasma emission field by 6–8 and illuminate fibers at f/1.5–f/1.7. The lens assemblies are protected by boron nitride shielding, and the minimum distance between the rf limiter shadow and boron nitride is 2 cm.

Optical fibers transmit the plasma emission to photodetectors. The 40 m fibers have 1 mm diameter cores and provide 65% transmission at f/1.5. Each detection channel consists of nine fibers in a $3\times3$ square bundle secured in ferrules with 3.9 mm sides. Including packing losses, the bundles provide 45% transmission at f/1.5, and the bundle

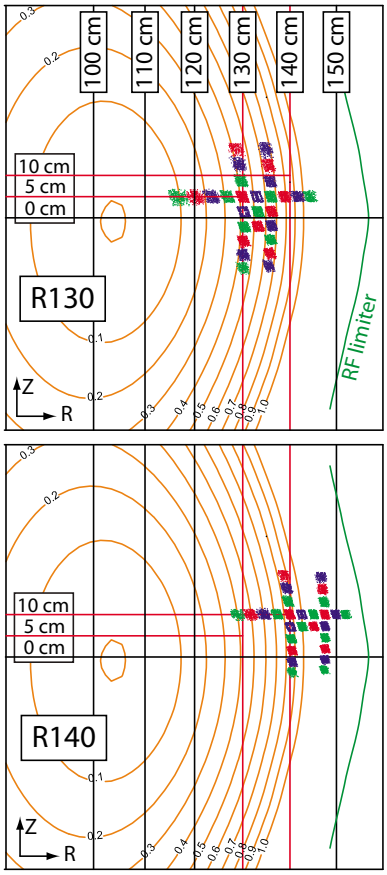


FIG. 3. (Color online) Initial channel layouts for R130 and R140 views on the center plane of the neutral beam with typical flux surfaces.

étendue is 2.3 $\mathrm{mm}^2$-ster. For comparison, BES fiber bundles on DIII-D provide 1.1 $\mathrm{mm}^2$-ster.[9] Aperture plates with strain relief hold fiber bundles at the image planes of the R130 and R140 lens assemblies. Both aperture plates hold 28 fiber bundles with 4.5 mm center-to-center spacing. Figure 3 shows the initial channel layouts for the R130 and R140 aperture plates. The channel patterns produce radial arrays, poloidal arrays, and 2D grids at the neutral beam, and the bundle spot sizes are 2–3 cm. The radial arrays provide coverage from $r/a \approx 0.1$ to beyond the last-closed flux surface.

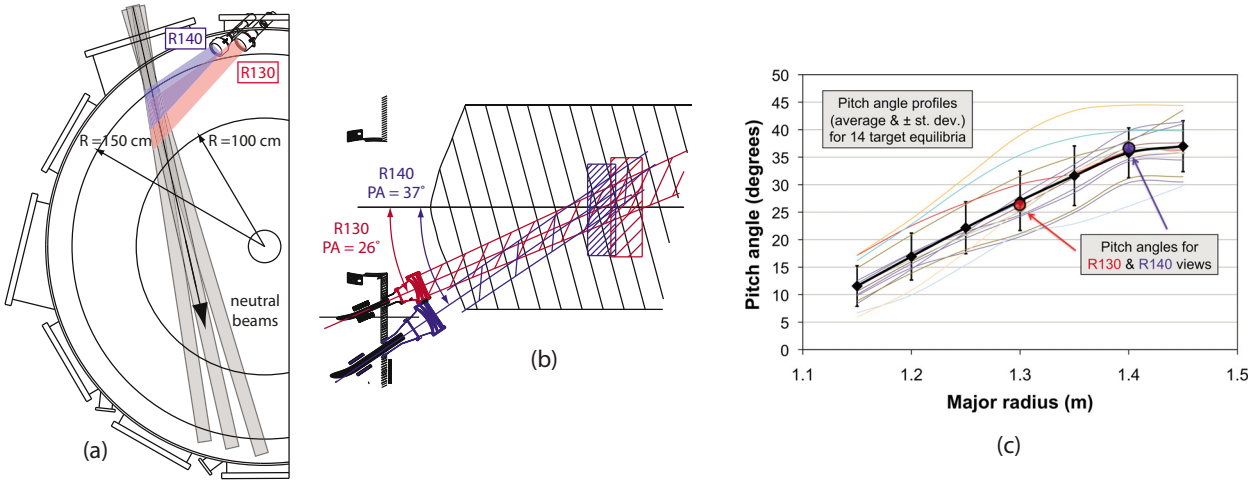


FIG. 2. (Color online) R130 and R140 viewing geometries: (a) plan view, (b) elevation view, and (c) pitch angle profile alignment.

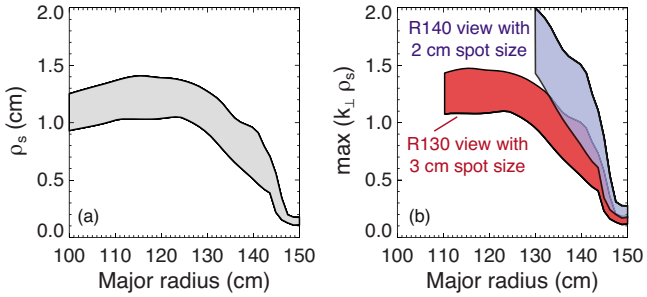


FIG. 4. (Color online) (a) Typical ion sound gyroradii ($\rho_s$) for NSTX H-mode plasmas and (b) maximum $k_\perp \rho_s$ values.

The four poloidal arrays are located at $r/a \approx 0.45$, 0.65, and 0.85 and in the scrape-off layer. The R130 view contains a $3 \times 3$ grid, and the R140 view contains a $2 \times 4$ grid.

Figure 4 illustrates the $k$-space measurement capabilities of the BES system. Typical ion gyroradii in NSTX H-mode plasmas are 1.0–1.5 cm in the core and 0.5–1.0 cm in the edge. With spot sizes approximately 3 cm in the core and 2 cm in the edge, the system is sensitive to modes with $k_\perp \rho_i \lesssim 1.5$ in both regions. As described in Ref. 10, accurate estimates of measurement parameters require point spread function and spatial transfer function calculations with atomic physics models.

The detection system is modular and expandable with eight-channel optics and detector modules. The optics module filters the plasma emission. Interference filters selectively pass neutral beam $D_\alpha$ emission while blocking other plasma emission. The filters are centered at 660.8 nm with a 3.9 nm full width at half maximum bandwidth, so the filters nominally block C-II emission lines. If the neutral beam $D_\alpha$ emission dominates the C-II emission, then the filters can be tilt-tuned to lower wavelength to capture $D_\alpha$ emission from 1/2 and 1/3 energy beam components. Finally, f/1.1 lenses collimate light for the filter, and f/0.58 aspheric lenses focus filtered light onto photodiodes.

## III. DETECTOR DESIGN AND AUXILIARY SYSTEMS

Each detector module contains eight photodetectors and filter spectrometers. The photodetectors are cooled to about −20 °C under vacuum. The condenser lenses described above sit at the vacuum interface. References 5 and 9 describe the prior BES photodetectors, and Reference 6 describes the new generation photodetectors employed here. To minimize amplifier noise, photodetectors employ surface-mount components to minimize input capacitance and optimized circuit board layout to minimize stray capacitance. A PIN photodiode (PDB-C164, Advanced Photonics) converts $D_\alpha$ emission into photocurrent, and a JFET (Phillips BF862) transimpedance amplifier converts the photocurrent to voltage. Next, a frequency compensation stage provides high frequency gain to generate a flat gain profile over the measurement bandwidth. The overall sensitivity is 4.5 mV/nW. The photodetectors achieve dark noise levels similar to prior BES photodetectors with only refrigerant cooling, not cryogenic cooling.

A signal conditioning unit between the detector module and digitizer distributes power to the detector module and provides adjustable gain and dc offset to utilize the full dynamic range of the digitizer. Differential signals are maintained from photodetectors to the digitizer. The digitizer is the D-tAcq ACQ132 with a field-programmable gate array configured as a finite impulse response (FIR) filter with 501 taps. The input sample rate is 32 MS/s, and the output sample rate is 2 MS/s. The FIR filter inhibits high frequency amplifier noise aliasing to lower frequency. The 1 MHz Nyquist frequency is adequate to study turbulent fluctuations with large Doppler shifts from high toroidal rotation in NSTX and Alfvén/energetic particle modes.

Finally, the auxiliary system includes a vacuum pump, a circulating chiller, and a programmable automated controller with digital input/output, analog input, relays, and thermocouples. The controller provides remote control capabilities for the circulating chiller and signal conditioning unit, and LABVIEW™ virtual instruments provide the control interface.

## ACKNOWLEDGMENTS

This work was supported by the U.S. Department of Energy under Grant Nos. DE-FG02-89ER53296, DE-SC0001288, and DE-AC02-09CH11466.

[1] R. J. Fonck, P. A. Duperrex, and S. F. Paul, Rev. Sci. Instrum. **61**, 3487 (1990).
[2] M. Ono, S. M. Kaye, Y.-K. M. Peng, G. Barnes, W. Blanchard, M. D. Carter, J. Chrzanowski, L. Dudek, R. Ewig, D. Gates, R. E. Hatcher, T. Jarboe, S. C. Jardin, D. Johnson, R. Kaita, M. Kalish, C. E. Kessel, H. W. Kugel, R. Maingi, R. Majeski, J. Manickam, B. McCormack, J. Menard, D. Mueller, B. A. Nelson, B. E. Nelson, C. Neumeyer, G. Oliaro, F. Paoletti, R. Parsells, E. Perry, N. Pomphrey, S. Ramakrishnan, R. Raman, G. Rewoldt, J. Robinson, A. L. Roquemore, P. Ryan, S. Sabbagh, D. Swain, E. J. Synakowski, M. Viola, M. Williams, J. R. Wilson, and NSTX Team, Nucl. Fusion **40**, 557 (2000).
[3] G. R. McKee, R. J. Fonck, D. K. Gupta, D. J. Schlossberg, M. W. Shafer, C. Holland, and G. Tynan, Rev. Sci. Instrum. **75**, 3490 (2004).
[4] G. R. McKee, R. J. Fonck, M. Jakubowski, K. H. Burrell, K. Hallatschek, R. A. Moyer, W. Nevins, D. L. Rudakov, and X. Xu, Plasma Phys. Controlled Fusion **45**, A477 (2003).
[5] R. J. Fonck, R. Ashley, R. Durst, S. F. Paul, and G. Renda, Rev. Sci. Instrum. **63**, 4924 (1992).
[6] N. Schoenbeck, S. Ellington, R. Fonck, K. Jaehnig, G. McKee, D. Smith, I. Uzun-Kaymak, and G. Winz, Rev. Sci. Instrum. **81**, 10D718 (2010).
[7] F. M. Levinton and H. Yuh, Rev. Sci. Instrum. **79**, 10F522 (2008).
[8] M. Podesta, W. W. Heidbrink, R. E. Bell, and R. Feder, Rev. Sci. Instrum. **79**, 10E521 (2008).
[9] D. K. Gupta, R. J. Fonck, G. R. McKee, D. J. Schlossberg, and M. W. Shafer, Rev. Sci. Instrum. **75**, 3493 (2004).
[10] M. W. Shafer, R. J. Fonck, G. R. McKee, and D. J. Schlossberg, Rev. Sci. Instrum. **77**, 10F110 (2006).